A Redox Role for the [4Fe4S] Cluster of Yeast DNA Polymerase δ

Phillip L. Bartels[1], **Joseph L. Stodola**[2], **Peter M.J. Burgers**[2,*], and **Jacqueline K. Barton**[1,*]

[1]Division of Chemistry and Chemical Engineering, California Institute of Technology, Pasadena, CA

[2]Department of Biochemistry and Molecular Biophysics, Washington University School of Medicine, St. Louis, MO

Abstract

A $[4Fe4S]^{2+}$ cluster in the C-terminal domain of the catalytic subunit of the eukaryotic B-family DNA polymerases is essential for the formation of active multi-subunit complexes. Here we use a combination of electrochemical and biochemical methods to assess the redox activity of the $[4Fe4S]^{2+}$ cluster in *Saccharomyces cerevisiae* polymerase (Pol) δ, the lagging strand DNA polymerase. We find that Pol δ bound to DNA is indeed redox-active at physiological potentials, generating a DNA-mediated signal electrochemically with a midpoint potential of 113 ± 5 mV versus NHE. Moreover, biochemical assays following electrochemical oxidation of Pol δ reveal a significant slowing of DNA synthesis that can be fully reversed by reduction of the oxidized form. A similar result is apparent with photooxidation using a DNA-tethered anthraquinone. These results demonstrate that the [4Fe4S] cluster in Pol δ can act as a redox switch for activity, and we propose that this switch can provide a rapid and reversible way to respond to replication stress.

For Table of Contents Only
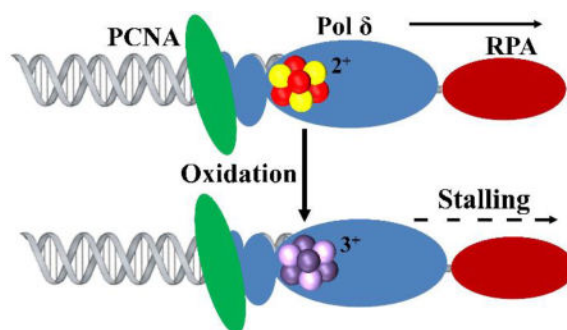
*to whom correspondence should be addressed at burgers@wustl.edu and jkbarton@caltech.edu.

INTRODUCTION

During genomic replication, eukaryotic cells divide the task of DNA synthesis between three B-family DNA polymerases (Pols): Pol α, Pol δ, and Pol ε (1). Each of these enzymes forms a multi-subunit complex composed of a catalytic subunit and a B-subunit, with additional accessory subunits present in Pol δ and Pol ε (2). Recent work has shown that a $[4Fe4S]^{2+}$ cluster in the C-terminal domain (CTD) of the catalytic subunit is essential for the formation of multi-subunit complexes in the case of Pol δ (3). Functionally, the B-family polymerases are believed to carry out DNA synthesis in a division of labor model, with the DNA primase-Pol α complex initiating 5′-3′ DNA synthesis by forming an RNA-DNA hybrid primer that is then extended by Pol ε on the continuously generated leading strand and by Pol δ on the discontinuously formed lagging strand (4). Additional roles for Pol δ during leading strand replication have been suggested (5, 6). Pol δ is also involved in various DNA recombinatorial and repair processes (7).

While the C-terminal [4Fe4S] cluster clearly plays a role in complex formation (3), several lines of evidence suggest a more direct functional role. First, a 2.5 Å X-ray crystal structure of the yeast Pol α CTD in complex with its B-subunit contained zinc in place of a cluster, demonstrating that structural integrity can be supported by simpler metals (8). Given the metabolic expense of [4Fe4S] cluster biosynthesis and loading into target proteins, the strict conservation of this cofactor in the B-family polymerases suggests that it serves an important function (9). Indeed, the importance of [4Fe4S] clusters in these enzymes is emphasized by the presence of an additional cluster in the unique Pol ε N-terminal domain (10).

The [4Fe4S] clusters perform a wide range of roles in biology including enzymatic catalysis and electron transfer (11). In the DNA polymerases, the cluster is not required for catalysis (3, 12). Many DNA-processing enzymes have now been shown to contain [4Fe4S] clusters, and, in many cases, a DNA-bound redox activity of the cluster has been demonstrated (13–16). These diverse proteins include base excision repair glycosylases, repair helicases and DNA primase. As in the Pol δ holoenzyme, the clusters are largely redox-inert in the absence of DNA (17–20). However, when bound to DNA, these protein cofactors undergo a significant negative shift in redox potential, activating the clusters toward oxidation (21–23). Electrochemical experiments with DNA-bound proteins show a reversible redox signal with potentials ranging from 65–95 mV versus the normal hydrogen electrode (NHE) (13–16). EPR studies support the assignment of the reversible signal to the $[4Fe4S]^{3+/2+}$ couple favored by high-potential iron proteins (HiPIP) that are electron carriers (13, 24–25). In addition to modulating redox potential, the π-stacked base pairs of DNA can act as a medium for long-range charge transport between redox-active proteins (26). DNA-mediated charge transport (DNA CT) is characterized by a shallow distance dependence and high sensitivity to base pair stacking, making it an excellent reporter of DNA integrity (26). Importantly, although DNA CT can be attenuated by proteins that bend the duplex or flip out bases, DNA CT can proceed unimpeded through nucleosome-wrapped DNA (26).

The redox activity of the [4Fe4S] cluster appears to be utilized in many of these proteins as a switch to regulate DNA binding and therefore activity. For the DNA repair enzyme,

Endonuclease III (EndoIII), the negative shift in redox potential associated with DNA binding has been shown to lead to a 500-fold increase in DNA affinity for the oxidized $[4Fe4S]^{3+}$ cluster versus the reduced 2+ form (27). In the case of human DNA primase, the oxidation state of the [4Fe4S] cluster also controls template binding, and redox switching through electron transfer between clusters in primase and Pol α has been proposed to regulate RNA primer handoff (16).

Here we focus on Pol δ, a central B-family polymerase. We utilize a combination of electrochemical, spectroscopic, and biochemical techniques to investigate redox activity in this enzyme and to understand the consequences of redox switching for polymerase activity. These studies provide a new perspective on polymerase regulation under oxidative stress.

MATERIALS and METHODS

Protein expression and purification

Yeast Pol δ (WT and exo⁻ D520V), RFC, RPA, PCNA, and *E. coli* EndoIII were expressed according to previously published protocols (3,28).

DNA preparation

The DNA substrate for electrochemistry consisted of a 49:58-mer primer-template composed of three oligomers: a 20-mer with a 3′ thiol modification, a 38-mer, and a 49-mer complement; sequences are as follows (see also Figure 1c):

> 20-mer Thiol: 5′ - GCT GTC GTA CAG CTC AAT GC - 3′ - $(CH_2)_2O(CH_2)_3SH$

> 38-mer: 5′ - TAA CAG GTT GAT GCA TCG CGC TTC GGT GCT GCG TGT CT - 3′

> 49-mer: 5′ - GCA TTG AGC TGT ACG ACA GCA GAC ACG CAG CAC CGA AGC GCG ATG CAT C - 3′

The bold G of the 49-mer was changed to an A or an abasic (AP) site for CA mismatch and abasic site discrimination experiments.

DNA replication assays used single-stranded M13mp18 plasmid purchased from New England Biolabs (NEB). Primers were purchased from IDT and purified by HPLC as described above. Primed DNA was formed by heating a 1:1 plasmid/primer mix in activity buffer (50 mM Tris-HCl, pH 7.8, 50 mM NaCl) to 90° C for 5′ and cooling to RT over several hours. The M13mp18 DNA primer had the following sequence (complementary to positions 6265-6235):

> 5′ - GAC TCT AGA GGA TCC CCG GGT ACC GAG CTC G - 3′

Primers were radiolabeled by incubating 10 pmol of 31-mer M13mp18 primer with T4 polynucleotide kinase (PNK) and [γ-^{32}P] ATP (Perkin Elmer) in T4 buffer (NEB) for 15 minutes at 37° C. Reactions were stopped by addition of EDTA to 10 mM and heating at 75° C for 10 minutes. 2 log DNA ladder (NEB) was dephosphorylated by calf intestinal alkaline phosphatase (CIAP; 60 minutes, 37° C) prior to labeling in the same manner. As an additional size standard, duplexed M13mp18 DNA was linearized by digestion with HincII

(60 minutes, 37° C) and dephosphorylated by CIAP prior to radiolabeling. Proteins and unincorporated ATP were removed using spin columns (BioRad Microspin6) equilibrated in Pol δ activity buffer (50 mM Tris-HCl, pH 7.8, 50 mM NaCl). T4 PNK, CIAP, HincII, and dsM13mp18 DNA were purchased from NEB.

Pol δ Electrochemistry

All electrochemical experiments were performed using a potentiostat equipped with a multiplexer, both from CH Instruments. Experiments used a standard 3-electrode cell composed of an Au working electrode, a Ag/AgCl reference electrode in 3 M NaCl (BASInc), and a 1 mm diameter Pt wire counter electrode (Lesker). Potentials were converted from Ag/AgCl to NHE by adding 212 mV to the potential as measured by Ag/AgCl; this correction accounted for both ambient temperature and the use of 3 M NaCl for reference storage (29). Experiments with Pol δ were all run in polymerase storage buffer (30 mM HEPES, pH 7.4, 350 mM NaAc, 1 mM DTT, 0.1 mM EDTA, 10% glycerol v/v, and 0.01% w/v decaethylene glycol monododecyl ether).

Because PCNA can slide directly onto DNA with open ends, the clamp loader complex RFC was excluded from these experiments (30). WT Pol δ 3′-5′ exonuclease activity was prevented by excluding Mg^{2+} from the buffer. In initial experiments, 3–5 μM WT Pol δ or exonuclease-deficient Pol δ D520V (DV) (31) was incubated on the electrode for several hours in the presence of 5–10 μM PCNA. To spare enzyme, later experiments used Pol δ DV at 500 nM in combination with 5.0 μM PCNA, 80 μM dATP and 8 mM $MgAc_2$. Cyclic voltammetry (CV; 100 mV/s scan rate) and square wave voltammetry (SQWV; 15 Hz frequency, 25 mV amplitude) scans were taken once per hour for several hours. Between scans, electrodes were covered in Parafilm and stored in a humid environment to minimize evaporation. CV scan rate dependence was assessed after 3 hours using rates of 20, 50, 80, 100, 200, 500, 750, and 1000 mV/s. In experiments with abasic and CA mismatch DNA, signal attenuation was calculated as follows:

$$[1 - ((\text{peak area on abasic or CA mismatch DNA})/(\text{peak area on unmodified DNA}))] \quad (1)$$
$$* 100\%$$

Pol δ concentrations are reported as the concentration of [4Fe4S] cluster, determined by UV-visible absorbance at 400 nm (ε_{400} = 13000 $M^{-1}cm^{-1}$) (3). The [4Fe4S] cluster loading was in the range of 70–85%, determined by dividing [4Fe4S] concentration by total protein concentration as measured by Bradford assay, Pierce BCA assay, and UV-visible absorbance at 280 nm (ε_{280} = 194100 $M^{-1}cm^{-1}$; estimated using the EXPasy ProtParam tool). Bradford and BCA assay standard curves were generated using a BSA standard, and both kits were purchased from Thermo Scientific. UV-visible spectra were taken on a Cary Varian instrument using 100 μL quartz cuvettes purchased from STARNA Cells.

When possible, diffusion coefficients were obtained from the scan rate dependence of the CV current using the Randles-Sevcik equation (32):

$$I_p = [0.4463(F^3/RT)^{1/2}](n^{3/2})(A)(D^{1/2})(C°)\nu^{1/2} \quad (2)$$

I_p is the peak current in amperes, F is Faraday's constant (96485 C·mol^{-1}), R is the universal gas constant (8.314 J·(mol·K)$^{-1}$), T is temperature in K, n is the number of electrons transferred per CV peak, A is electrode area in cm^2, D is the diffusion coefficient in cm^2·s^{-1}, C° is bulk protein concentration in mol·cm^{-3}, and ν is the scan rate in V·s^{-1}. Experimental values of D were compared to those estimated by the Stokes-Einstein equation,

$$D = k_B T/6\pi\eta R \quad (3)$$

where k_B is Boltzmann's constant (1.38 × 10^{-23} J·K^{-1}), T is the incubation temperature (293 K), η is the solution viscosity (estimated to be 1.38 × 10^{-3} Pa·s for an aqueous solution with 10% glycerol), and R is the hydrodynamic radius. R was estimated to be ~26 Å from dimensions obtained from X-ray crystal structures of DNA-bound Pol3, Pol1–Pol12, and PCNA (PDB ID 3IAY, 3FLO, and 4YHR, respectively).

Electrochemical Oxidation and Spectroscopic Analysis of Pol δ

To prevent cluster degradation in the presence of O$_2$, bulk electrolysis was performed in an anaerobic glove bag (COY) under a 95% N$_2$, 5% H$_2$ atmosphere with an O$_2$-scavenging catalyst present. Buffers were degassed by bubbling in argon for several hours and stored open in the glove bag overnight prior to experiments. For spectroscopic characterization, a 150 μL sample of 1–2 μM Pol δ was added to two identical DNA-modified electrodes. On one electrode, a potential of 0.412 V vs NHE was applied for ~15 minutes, while no potential was applied to the other. Oxidation yields were estimated by taking the difference between the total charge obtained in the presence of Pol δ and that generated by electrolysis with buffer alone. Following electrolysis, UV-visible and electron paramagnetic resonance (EPR) spectroscopy were used to confirm the integrity of the cluster after electrolysis. Samples were sealed in cuvettes for UV-visible spectroscopy, and subsequently returned to the glove bag and added to EPR tubes. Tubes were sealed by Parafilm and frozen in liquid nitrogen outside the bag. Continuous wave X-band EPR was performed at 10 K, and each experiment consisted of 9 sweeps taken at 12.88 mW microwave power, 2 G modulation amplitude, and 5.02 × 10^3 receiver gain.

Pol δ Activity Assays

Immediately prior to assays, Pol δ DV was oxidized on Au rod electrodes exactly as described for spectroscopic characterization, but the sample was diluted to 190 nM in degassed storage buffer in a total volume of 30–40 μL. Reduction of oxidized sample was carried out at a potential of −0.188 V vs NHE for a similar length of time. In parallel with electrolysis, 140 μL reaction mixes (0.1mg/mL BSA, 80 μM each dNTP, 500 μM ATP, 2.0 nM M13mp18 with a ^{32}P-labeled primer, 8.0 mM MgAc$_2$, 500 nM RPA, 5.0 nM RFC and 5.0 nM PCNA, 50 mM NaCl, 50 mM Tris-HCl, pH 7.8) were prepared inside the glove bag. The PCNA sliding clamp was loaded onto the primer end by incubating the reaction mix

with the RFC clamp loader and ATP for 1 minute at 30 °C. After clamp loading, reactions were initiated by the addition of 2 nM (final concentration) oxidized, untreated, or re-reduced Pol δ DV. Reactions were run at 30 °C, and 20 μL aliquots were removed and quenched at specific time points by adding 10 μL stop mix (10 mM EDTA and 0.1% v/v SDS final concentration). The polymerase was heat-inactivated for 10–20 minutes (55 °C), and samples were counted on a liquid scintillation counter to determine exposure time (1 hour per 300,000 counts). Samples were dried on a speed vacuum and dissolved in alkaline gel buffer (500 mM NaOH, 10 mM EDTA) with 1× alkaline loading dye (6× stock: 300 mM NaOH, 6.0 mM EDTA, 18% Ficoll w/v, 0.25% xylene cyanol w/v, and 0.15% bromocresol green w/v), and equivalent amounts of radioactivity were then loaded onto a 1% alkaline agarose gel and run at 30 V for 14–15 hours. Gels were neutralized in 7% TCA (w/v) in water for 30 minutes at RT and dried under mild pressure for several hours, exposed on a phosphor screen and visualized on a Typhoon phosphorimager (GE Healthcare). Products were analyzed using ImageQuant software (GE Healthcare). The relative amounts of DNA synthesis were determined by dividing the volume of the largest band in an oxidized sample by the equivalent band in the appropriate untreated sample.

To limit DNA synthesis to that of a single processive cycle by the PCNA-Pol δ complex, 0.01 mg/mL heparin was included in reactions (33) that were then analyzed on 5% polyacrylamide gels. In these instances, Pol δ was added after clamp loading and reactions were started by adding a mix of dNTPs and heparin. Quenched reactions were then counted, dried, and redissolved in 2.0 μL formamide loading dye. Immediately prior to gel loading, samples were heated at 90 °C for 10 minutes, and gels were run at ~50 W for 5 hours in 1× TBE buffer. Polyacrylamide gels were then exposed and imaged by phosphorimager analysis.

Tris-HCl, NaCl, $MgAc_2$, BSA, and heparin were purchased from Sigma-Aldrich, while dNTPs and ATP were from NEB. dNTPs, ATP, and $MgAc_2$ were thoroughly degassed prior to reaction, and the protein stocks were kept open during a series of vacuum/nitrogen/gas mix purges to minimize residual oxygen.

Chemical Oxidation of Pol δ

For photooxidation, the 31-mer M13mp18 primer was covalently modified with a 5′ anthraquinone (AQ). AQ was prepared as a phosphoramidite and added to the unmodified DNA on a DNA synthesizer according to previously reported procedures (34). The presence of AQ was verified by MALDI-TOF, and the modified primer was annealed to M13mp18 DNA in Pol δ activity buffer (50 mM Tris-HCl, pH 7.8, 50 mM NaCl). Because the 5′ AQ modification prevented ^{32}P end-labeling, DNA was labeled by adding 2 μCi [α-^{32}P] dATP (Perkin Elmer) to the reaction, and incorporation of [α-^{32}P] dATP was facilitated by lowering the concentration of cold dATP from 80 μM to 10 μM.

Anaerobic reaction mixes lacking dNTPs were prepared in glass vials and incubated under a solar simulator equipped with a UVB/C long pass filter or in the dark for 30 minutes. To ensure complete oxidation, 2-fold molar excess of both PCNA and Pol δ DV were included. As controls, reactions were also run using unmodified DNA (no AQ) and AQ reactions were repeated with 140 nM Klenow fragment exo⁻ (NEB). After treatment, samples were

returned to the glove bag and transferred into Eppendorf tubes containing dNTPs to start the reaction. Free dNTPs were removed using BioRad Microspin 6 columns in SCC buffer (GE Healthcare) and sample radioactivity was quantified on a liquid scintillation counter. Samples were then run out on a 1% alkaline agarose gel and visualized by phosphorimaging analysis. Overall [α-^{32}P] dATP incorporation was used to compare overall DNA synthesis levels by dividing the total radioactivity counts in oxidized samples by those of dark controls.

RESULTS

Electrochemical Characterization of Pol δ

To determine whether Pol δ holoenzyme was redox active in the presence of DNA, we carried out electrochemistry on DNA-modified gold electrodes. In initial experiments, 3 μM WT Pol δ in storage buffer was combined with 10 μM PCNA and incubated on the electrode for several hours. CV scans taken hourly reveal a reversible signal with a midpoint potential of 116 ± 3 mV vs NHE (Figure 1a). This signal grows in over time to reach a maximum size of 41 ± 4 nC and -51 ± 2 nC for the reductive and oxidative peaks at a 100 mV/s scan rate after two hours of incubation (Figure 1). The CV current varies linearly with the square root of the scan rate (Figure S1), as expected of a diffusive rather than adsorbed species (32). The diffusive nature of the signal is in agreement with earlier studies of DNA binding proteins (14). No differences were observed between aerobic and anaerobic electrochemistry carried out in a glove bag, indicating that the cluster is relatively stable in air and consistent with the general long-term stability of B-family DNA polymerases (35). The redox couple observed was attributed to the [4Fe4S]$^{3+/2+}$ based on the fact that Pol δ is HiPIP-like, being EPR-silent unless oxidized (3). In addition, the electrochemical signal is similar to the DNA glycosylases EndoIII and MutY, in which the identity of the couple has been established by EPR (13, 24).

We could obtain quantifiable signals at lower concentrations by adding dNTPs and Mg^{2+} to enhance protein association with the DNA. To prevent degradation of the DNA substrate by the 3′-5′ exonuclease activity of WT Pol δ, we turned to the exonuclease-deficient mutant Pol δ DV (D520V) for these experiments (31). At 113 ± 5 mV vs NHE, the midpoint potential of Pol δ DV is indistinguishable from WT (Figure 1, S3). By adding 80 μM dATP (the incoming nucleotide), 8.0 mM MgAc$_2$, and 5.0 μM PCNA, we were able to see signals with Pol δ concentrations as low as 500 nM (Figure 1). Under these conditions, the maximum CV peak areas were 6.9 ± 1 nC and -7.5 ± 1 nC for the reductive and oxidative peaks at a scan rate of 100 mV/s.

The midpoint potential of Pol δ is within the HiPIP potential regime, but it is slightly higher than the 65–95 mV vs NHE reported for DNA-bound repair proteins (13, 28). We used the well-studied *E. coli* BER glycosylase EndoIII (28) to determine if the measured potential is truly distinct or the result of different buffer conditions. In our standard phosphate buffer (20 mM sodium phosphate, pH 7.5, 100 mM NaCl, 1 mM EDTA, 10% glycerol v/v), the EndoIII midpoint potential is ~80 mV versus NHE (28). However, when we exchanged EndoIII into Pol δ storage buffer, CV and SQWV carried out with 140 μM or 1.5 μM EndoIII result in a midpoint potential of 113 ± 3 mV versus NHE, which is indistinguishable

from Pol δ (Figure S2b). UV-visible spectra confirm the stability of EndoIII in Pol δ buffer (Figure S2a). The observed increase in EndoIII potential is most likely due to the significantly higher ionic strength of Pol δ storage buffer (350 mM NaAc in Pol δ buffer vs 150 mM NaCl in EndoIII buffer) (36, 37). In any case, the fact that the EndoIII and Pol δ redox potentials are indistinguishable under identical buffer conditions supports the assertion that the [4Fe4S] cluster resides in the same narrow potential regime in both proteins.

Given that Pol δ ordinarily functions in complex with PCNA, we next asked what effect PCNA might have on the electrochemical properties of Pol δ. In the absence of PCNA, the midpoint potential is unaltered at 115 ± 8 mV versus NHE, but the signal was markedly smaller, reaching a maximum CV peak area of 0.4 ± 0.1 nC for the reductive peak and −0.7 ± 0.1 nC for the oxidative peak (Figure S3). The signal also decays more rapidly with PCNA absent, suggesting lower polymerase stability in the absence of PCNA. To compare the signals with and without PCNA more quantitatively, diffusion coefficients (D) under both conditions were calculated using the Randles-Sevcik equation (32). At maximum signal size, D was found to be $6.7 ± 3 \times 10^{-6}$ cm$^2 \cdot$ s^{-1} with PCNA and dATP present, which is within one order of magnitude of an estimate (6.0×10^{-7} cm$^2 \cdot$ s^{-1}) based on the Stokes-Einstein equation. The difference between these values most likely reflects errors from the use of multiple partial crystal structures to estimate the hydrodynamic radius. In the absence of PCNA, D decreases to $1.2 ± 0.3 \times 10^{-7}$ cm$^2 \cdot$s^{-1}, which is on the same order of magnitude as the value estimated from the Stokes-Einstein equation. These results are consistent with differently shaped complexes, in agreement with the known elongate form of Pol δ alone in solution and the more compact form expected when multiple subunits have engaged with PCNA (3, 38). To see if dNTPs contribute to the shape of PCNA-bound Pol δ, we prepared a surface with Pol δ and PCNA but lacking dATP and Mg^{2+}. Under these conditions, the signal is comparable to that in the absence of PCNA, giving a D value of $2.2 ± 0.7 \times 10^{-7}$ cm$^2 \cdot$ s^{-1}. Taken together, these results indicate that PCNA does not affect the potential of Pol δ but is critical for effective DNA binding, and the entire complex is more likely to remain DNA-bound when dNTPs are present.

To determine if the Pol δ signal is DNA-mediated, we carried out electrochemistry using DNA containing either an abasic site or a CA mismatch 6 nucleotides from the thiolated end (Figure 1c). In addition to base stack integrity, DNA-mediated signaling in proteins is dependent on film morphology, with DNA-bound proteins capable of charge transport both through the DNA bases and directly through the monolayer surface (Figure S4) (28). In general, closely packed monolayers provide more DNA which may be less accessible to large proteins, while the opposite is true of loosely packed monolayers. To address all of these issues together, we prepared monolayers in the presence of 100 mM MgCl$_2$ to form closely packed islands of DNA (30–50 pmol·cm^{-2}) in parallel with standard loosely packed monolayers (15–20 pmol·cm^{-2}) formed without Mg^{2+} (Figure S4) (39, 40). For both morphologies, half of each chip contained well-matched DNA, and the other half contained either abasic or CA mismatch DNA (Figure S4a). In all experiments, we used 500 nM Pol δ DV in the presence of PCNA, dATP, and MgAc$_2$.

Consistent with previous studies on EndoIII (28), Pol δ redox potentials are identical on both film morphologies, supporting the assertion that all observed signals are from DNA-bound

proteins (Figure S4). On closely packed DNA films, signal size is highly variable, but 46 ± 33% signal attenuation as determined by SQWV was observed on abasic DNA (Figure S4). No mismatch discrimination was observed, and even the abasic site discrimination decreased over time as more protein diffused to the surface. In general, the signals on closely packed monolayers are consistent with variable DNA accessibility and significant steric hindrance causing protein-DNA complexes to lie flat on the surface (Figure S4). In contrast, loosely packed monolayers show very consistent signal sizes and significant charge attenuation on both DNAs containing abasic sites and CA-mismatches, reaching a maximum of 44 ± 16% on abasic DNA and 46 ± 29% on CA-mismatch DNA after 2 hours of incubation as measured by SQWV (Figure 1, Figure S4). Abasic site and mismatch discrimination also remain stable over time, indicating that DNA accessibility and steric hindrance are not significant problems on loosely packed DNA. Together, these results confirm that Pol δ is capable of DNA-mediated signaling and emphasize the importance of substrate accessibility when assessing CT by large protein complexes.

Activity Assays with Oxidized and Reduced Pol δ

Having seen that DNA binding can activate Pol δ for redox activity, we next asked how the cluster oxidation state might affect polymerase activity. As purified, Pol δ exists largely in the $[4Fe4S]^{2+}$ state (3), so any assessment of activity differences would require extensive oxidation to generate sufficient amounts of the $[4Fe4S]^{3+}$ cluster for comparison. To this end, we turned to bulk electrolysis on DNA-modified electrodes, applying an oxidizing potential of 0.412 V verses NHE for 15–20 minutes.

To prevent aerobic degradation of oxidized cluster, all experiments were performed in a glove bag under a 95% N_2/5% H_2 atmosphere.

To achieve high yields, bulk electrolysis is best done on an electrode with a relatively large surface area. Multiplexed chips have many advantages for electrochemical characterization, but only a single electrode can be addressed at a time and each sample in a quadrant is distributed between 4 electrodes. To overcome these limitations, we switched to single gold rod electrodes for these experiments. In order to characterize this system, a sample of concentrated (150 μL of 2.74 μM) Pol δ was oxidized on a DNA-modified electrode in a custom-made glass cell for several hours (Figure S5a, b). UV-visible spectra were taken before and after electrolysis, after which the sample was then frozen for EPR in parallel with untreated protein (Figure S5c, d). The [4Fe4S] cluster oxidation generally results in a broad increase in UV-visible absorbance from 300–450 nm with a less distinct peak at 410 nm in both the $[4Fe4S]^{3+}$ and $[3Fe4S]^{+}$ species (41–43). After bulk electrolysis, increased absorbance from 300–400 nm, consistent with cluster oxidation, was indeed observed. No significant increase in absorbance at 800 nm occurred after oxidation, and the 280 nm peak associated with aromatic and thiolated amino acid residues remained distinct. From our own observations, protein aggregation tends to generate a U-shaped curve with high absorbance at 800 nm and a shallow, poorly defined peak at 280 nm, and the lack of these features in our spectra indicate that oxidized Pol δ did not aggregate (Figure S5c). EPR signals are small as a result of the low sample concentration, but clear signals at g = 2.08 and g = 2.02 are present in the oxidized sample (Figure S5d). These signals are consistent with a combination

of $[4Fe4S]^{3+}$ and $[3Fe4S]^+$ cluster oxidation products (24, 42–43). A smaller signal at g = 2.02 was also present in the native sample, consistent with earlier reports of residual [3Fe4S] $^+$ cluster in untreated Pol δ (3). That some $[3Fe4S]^+$ cluster would occur upon oxidation is not surprising, and similar results have been obtained for EndoIII and MutY (13, 24). In earlier studies, loss of iron was attributed in part to damage incurred upon freezing, which may have also happened here. Furthermore, oxidized Pol δ was stored away from protective DNA long enough to take a UV-visible spectrum prior to freezing. In any case, some $[4Fe4S]^{3+}$ cluster was still observed, and the $[3Fe4S]^+$ cluster that did occur would have formed as a degradation product of the $[4Fe4S]^{3+}$ cluster (13).

Because activity assays require only low nanomolar polymerase concentrations, bulk electrolysis for these experiments was carried out with 190 nm Pol δ DV to minimize sample waste. Oxidation yields under these conditions were higher, typically around 75 – 90% as determined from the total charge passed. After electrolysis, untreated or oxidized Pol δ DV was added directly to pre-made reaction mixes to a final concentration of 2 nM (Figure 2a). When run out on an alkaline agarose gel, it is apparent that at early time points less DNA synthesis was carried out by oxidized Pol δ (Figure 2b, S6a). DNA synthesis can be more quantitatively compared for the oxidized versus untreated sample by dividing the amount of frontier products (highest molecular weight major products) in the oxidized sample by the amount present in untreated samples. Using this analysis, oxidized Pol δ at 60–80% yield forms only 30–50% as many large (~ 5 kb) DNA products as untreated Pol δ after 30 seconds (Figure 2c). Significantly, higher oxidation yields lead to lower activity levels. In any case, this difference gradually decreases over the course of 10 minutes. Regardless of oxidation state, no DNA synthesis occurs in samples lacking PCNA, confirming that all observed DNA synthesis is processive (Figure S6c).

Reduction of the oxidized Pol δ stock by electrolysis at −0.188 V versus NHE effectively restores DNA synthesis, reaching 90% of untreated levels at early time points (Figure 2b, c, S6b). Critically, this result both confirms the reversibility of oxidative slowing and provides support for the $[4Fe4S]^{3+}$ cluster as the major oxidation product. As mentioned earlier, the reversible electrochemical signals are consistent with $[4Fe4S]^{3+/2+}$ cycling, but EPR spectroscopy with oxidized Pol δ showed evidence of both $[4Fe4S]^{3+}$ and $[3Fe4S]^+$ products in the sample, leading to some ambiguity. However, the nearly complete restoration of native activity levels upon re-reduction would not be expected if most of the cluster had degraded to the $[3Fe4S]^+$ state, supporting the $[4Fe4S]^{3+}$ cluster as the major oxidation product. These combined results thus indicate that the $[3Fe4S]^+$ cluster seen by EPR likely forms after the $[4Fe4S]^{3+}$ major product degrades over time in the absence of DNA; we have observed this previously with sample freezing for *E. coli* EndoIII and MutY following chemical oxidation (13, 24).

To gain further insight into the effect of oxidation, reaction rates were estimated by comparing frontier velocities. Velocities were calculated by dividing the amount of the largest quantifiable band of DNA by time and the number of polymerase molecules present (44). This method yields maximum rates of 118 ± 63 (SD, n = 7) nt/s per enzyme for untreated Pol δ and 21 ± 27 (SD, n = 5) nt/s for oxidized Pol δ at 2 minutes. The rates obtained for untreated Pol δ are consistent with previously published *in vitro* results (33),

while the oxidized form is significantly slower. This calculation represents just an upper estimate, as typical bulk electrolysis fails to oxidize around 20–30% of the enzyme; thus, some of the DNA synthesis observed in oxidized samples can be attributed to the non-oxidized population. Indeed, the comparable amounts of DNA synthesis observed after 5–10 minutes could have resulted from either slow oxidized polymerase catching up or redistribution by of residual native Pol δ in the oxidized sample. Overall, it is clear from these experiments that oxidation leads to a decrease in replication rate, but resolution on alkaline agarose gels is insufficient to distinguish between complete stalling or dramatic slowing of DNA synthesis.

To distinguish between stalling and slowing of DNA synthesis by oxidized Pol δ, reactions were analyzed on 5% polyacrylamide gels to obtain increased resolution in the 30–1000 nucleotides range. In addition, DNA synthesis was limited to that of a single processive cycle by the PCNA-Pol δ complex by adding heparin, which traps dissociated Pol δ (33). Without the heparin trap, products up to 7 kb were observed, due to multiple processive cycles of synthesis (Figure 2, S6). In order to visualize products at all sizes, reactions containing heparin were divided in two, with half loaded onto a polyacrylamide gel and half onto an alkaline agarose gel. With heparin present, alkaline agarose gels demonstrate a severe limitation to DNA synthesis, with no products larger than ~1 kb observed on alkaline agarose gels (data not shown). When these products are resolved on polyacrylamide gels, a greater proportion of both very small (~primer length) and very large (~1 kb) products are formed by untreated Pol δ, while the oxidized form generates more intermediate products between 30 and 1000 nucleotides (Figure S7).

These results illustrate several important points about the effects of oxidation on Pol δ DNA synthesis. First, they verify that the oxidized form remains active and does not completely stall. Second, the relatively greater amounts of very small products and unextended primers in reactions with native sample indicate greater susceptibility to dissociation from DNA and trapping by heparin, while the native form that does associate produces longer products. In contrast, oxidized Pol δ leaves fewer primers unextended or fully extended, instead making more intermediate products between 150 bp and 1 kb. The greater proportion of extended primers is consistent with tighter DNA binding after cluster oxidation, as has been observed with both primase and DNA repair proteins (16, 27). However, the slower procession indicates that tighter binding impedes rapid procession, acting as a brake on PCNA-mediated DNA synthesis. These experiments suggest that the similar activity levels observed on alkaline agarose gels at time points beyond 5 minutes could be explained by either the oxidized form gradually catching up or by redistribution of the residual native enzyme in the sample. Regardless of the precise details, the overall impact of polymerase stalling, with a 6-fold decrease in rate, would be significant on the timescale of S-phase; unperturbed yeast S-phase lasts ~30 minutes, while using oxidized Pol δ moving at 20 nt/s to replicate the lagging strand of the yeast genome would itself require 27 minutes (45–47).

Chemical Oxidation of Pol δ with Anthraquinone

Electrochemical oxidation provides clear advantages in estimating yields and re-reducing the oxidized sample, but the use of chemical oxidants is much more common. Thus, we were

interested to see if chemical oxidation could yield an equivalent result. To this end, we used an anthraquinone (AQ)-derived photooxidant covalently tethered to the 5′ end of the DNA primer (34, 48). AQ has the advantage of oxidizing samples in a DNA-mediated fashion instead of the less effective, direct oxidation of the protein by oxidants in solution (3, 48). Irradiation at 350 nm of AQ generates an excited triplet state capable of oxidizing DNA bases, and AQ has been studied extensively in the context of DNA CT (48–50). The DNA base of lowest potential, guanine, has a redox potential of 1.29 V, which is considerably higher than that of the Pol δ [4Fe4S] cluster at 113 mV (51). The presence of AQ on the primer, however, prevents 5′ ^{32}P end-labeling, so [α-^{32}P] dATP added to reactions was used as an alternative label (Figure 3a). Since [α-^{32}P] dATP is not necessarily incorporated in a 1:1 ratio with DNA-primed ends, activity levels were compared by total scintillation counts rather than by directly quantifying gel bands.

Following irradiation, samples with AQ showed lower overall DNA synthesis relative to identical samples kept in the dark (Figure 3b, c). As with electrochemistry, the maximum differentials occur at earlier time points. After 30 and 60 seconds, irradiated Pol δ showed 40–60% of dark control DNA synthesis. In contrast, reaction mixes irradiated in the presence of unmodified DNA are not significantly different from dark controls at early time points, and remain equal or greater throughout the time course (Figure 3c, S8). Similarly, no significant differences are observed between reactions with irradiated or untreated *E. coli* Klenow fragment exo⁻ on AQ-modified DNA (Figure S8), indicating that the attenuation observed in Pol δ DNA synthesis can be attributed to [4Fe4S] cluster oxidation. Assuming the activity differential at early time points approximated the percentage of oxidized sample, as was the case electrochemically, photooxidation yields ranged from 40–50%. Overall, the pattern of attenuated activity after photooxidation is consistent with the results from electrochemical experiments (Figure 3c), independently confirming the slowing of Pol δ upon cluster oxidation.

DISCUSSION

In this work, we have demonstrated that the [4Fe4S] cluster of DNA polymerase δ can serve an important functional role as a redox-active cofactor that regulates enzymatic activity. On DNA-modified gold electrodes, Pol δ shows a reversible signal with a midpoint potential of 113 ± 5 mV versus NHE. Notably, this potential is comparable to that of the previously characterized [4Fe4S] protein EndoIII under the same buffer conditions. Charge attenuation in the presence of either an abasic site or a CA mismatch confirms that the redox signal is DNA-mediated. Activity assays carried out with electrochemically oxidized Pol δ demonstrate that oxidation results in significant slowing of processive DNA synthesis; the same result occurs following irradiation in the presence of an anthraquinone photooxidant. An assessment of both large and small DNA products indicates that the oxidized form remains active, but it is less processive. Given the retention of activity with decreased processivity, these results are consistent with an increase in DNA binding affinity upon oxidation, which would impede rapid sliding of PCNA-bound Pol δ. A significant increase in DNA binding is evident also with EndoIII upon oxidation (27). Critically, reduction by bulk electrolysis largely restores activity to native levels, confirming that cluster oxidation acts as a reversible switch. The reversibility of oxidation also lends further support to our

electrochemical and spectroscopic evidence for the [4Fe4S]$^{3+}$ cluster as the biologically relevant oxidation product rather than degraded [3Fe4S]$^+$ cluster. Taken as a whole, these results suggest that reversible oxidation of the [4Fe4S] cluster in Pol δ could provide a rapid and reversible way to respond to replication stress.

Replication stress is a general term for fork slowing or stalling due to factors such as dNTP depletion, UV irradiation, and oxidative stress (52). Both replicative helicases and polymerases are known to be stabilized at stalled forks independently of checkpoint kinase activity, although the mechanism of stabilization and its relationship to global checkpoint regulation remains incompletely understood (53). Pol δ slowing through cluster oxidation would be a straightforward way to stall replication on the lagging strand, and this form of slowing could also complement more standard regulatory mechanisms. In general, Pol δ slowing would lead to accumulation of single-stranded DNA and RPA on the lagging strand, activating checkpoint kinases that could then stall the helicase by phosphorylation of key subunits (54, 55). Among other types of stress, oxidative stress and ionizing radiation carry a heightened risk of double strand break formation (56). Furthermore, reactive oxygen species generate lesions such as 8-oxoguanine (OxoG), which is highly mutagenic due to the propensity of replicative polymerases to generate OxoG:A mispairs (57). Oxidation of the [4Fe4S] cluster from the 2+ to 3+ form could either occur directly, by reactive oxygen species, or, more likely, by charge transport (CT) communication through double stranded DNA with other oxidized species. Previously, we have seen that guanine radicals, the precursors to OxoG, can carry out DNA CT to oxidize the [4Fe4S] cluster of DNA-bound EndoIII (24). An additional benefit of polymerase stalling by DNA-mediated oxidation would be the prevention of excessive DNA synthesis under high risk circumstances. In addition to preventing damage, redox signaling to and from Pol δ could play a role in fork reversal and recombination events associated with replication stress (52, 58).

A general model for redox regulation of Pol δ is shown in Figure 4. In this model, processive lagging strand replication proceeds until replications stress occurs and the Pol δ [4Fe4S]$^{2+}$ cluster is oxidized either directly or by an electron acceptor, possibly an oxidized [4Fe4S] protein or a guanine radical formed during oxidative stress. We have found, in the case of EndoIII, that cluster oxidation promotes a substantial increase in binding affinity (27). Here, given the already tight binding to DNA of Pol δ with PCNA, a still tighter binding causes Pol δ to slow its progression. The slowing of lagging strand synthesis would lead to RPA accumulation and an activation of checkpoint signaling, ultimately resulting in repair or replication fork collapse. Once the conditions of stress resolve, lagging strand synthesis can be restored by reduction of the Pol δ [4Fe4S]$^{3+}$ cluster, likely by another [4Fe4S] protein involved in DNA processing. Importantly, only Pol δ bound to the DNA in a complex with PCNA is readily oxidized, leaving the bulk of unbound Pol δ in the reduced 2+ form. Furthermore, this signaling can occur rapidly and at distance through DNA-mediated CT.

It is interesting to consider the many possible partners for DNA CT with Pol δ in the context of this model. First, Pol δ could be directly oxidized by species formed during oxidative stress, such as the guanine radical cation (24). After removal of reactive oxygen species, a partner [4Fe4S] protein could then re-reduce Pol δ and restore lagging strand replication. Alternatively, the entire redox cycle could be carried out between Pol δ and other [4Fe4S]

proteins associated with the replication fork. The nuclease-helicase Dna2 is a prime example of such a partner, as it associates with the replication fork and is involved in both fork reversal and double strand break repair (59, 60). In human cells, the [4Fe4S] DNA repair glycosylase MUTYH associates with PCNA during S-phase; whether this association also occurs in the yeast homologue, Ntg2, is not known (61). If the glycosylases do generally associate with the fork, redox signaling could enable rapid communication between replication and repair pathways in eukaryotes. Finally, redox signaling between Pol δ and the B-family translesion DNA synthesis polymerase Pol ζ could help these proteins to hand off DNA containing bulky lesions. Indeed, a role for the cluster in the Pol δ – Pol ζ switch has already been suggested (62). In this view, Pol δ and Pol ζ switch by exchanging their shared B-subunits, although this would leave the cluster vulnerable to degradation (63). However, a redox handoff similar to that suggested between primase and Pol α could allow such a transfer without requiring direct subunit exchange (16). While redox control of Pol δ would provide clear opportunities and is intriguing to consider, the *in vivo* mechanism and possible partners still require further investigation.

In summary, we have shown that Pol δ can use its [4Fe4S] cluster for reversible electron transfer along DNA and that oxidation of the cluster leads to reversible stalling. Taken together, our data suggest a model in which Pol δ uses redox signaling through DNA to sense oxidative stress, stalling replication under the mutagenic conditions, and potentially coordinating activities with repair and other replication proteins. Overall, the redox sensitivity of Pol δ reveals the oxidation state of the [4Fe4S] cluster to be a critical redox switch, and means rapidly and reversibly to respond to replication stress.

Supplementary Material

Refer to Web version on PubMed Central for supplementary material.

Acknowledgments

References

1. Lujan SA, Williams JS, Kunkel TA. Trends Cell Biol. 2016; 26:640–654. [PubMed: 27262731]

2. Johansson E, MacNeill SA. Trends Biochem. Sci. 2010; 35:339–347. [PubMed: 20163964]

3. Netz DJA, Stith CM, Stümpfig M, Köpf G, Vogel D, Genau HM, Stodola JL, Lill R, Burgers PMJ, Pierik AJ. Nat. Chem. Biol. 2012; 8:125–132.

4. Burgers PMJ, Kunkel TA. Annu. Rev. Biochem. 2017; 86:417–438. [PubMed: 28301743]

5. Johnson RE, Klassen R, Prakash L, Prakash S. Mol. Cell. 2015; 59:163–175. [PubMed: 26145172]

6. Yeeles JTP, Janska A, Early A, Diffley JFX. Mol. Cell. 2017; 65:105–116. [PubMed: 27989442]

7. Prindle MJ, Loeb LA. Environ. Mol. Mutagen. 2012; 53:666–682. [PubMed: 23065663]

8. Klinge S, Núñez-Ramírez R, Llorca O, Pellegrini L. EMBO J. 2009; 28:1978–1987. [PubMed: 19494830]

9. Netz DJA, Mascarenhas J, Stehling O, Pierik AJ, Lill R. Trends Cell Biol. 2014; 24:303–312. [PubMed: 24314740]

10. Jain R, Vanamee ES, Dzikovski BG, Buku A, Johnson RE, Prakash L, Prakash S, Aggarwal AK. J. Mol. Biol. 2014; 426:301–308. [PubMed: 24144619]

11. Johnson DC, Dean DR, Smith AD, Johnson MK. Annu. Rev. Biochem. 2005; 74:247–281. [PubMed: 15952888]

12. Swan MK, Johnson RE, Prakash L, Prakash S, Aggarwal AK. Nat. Struct. Mol. Biol. 2009; 16:979–986. [PubMed: 19718023]

13. Boal AK, Yavin E, Lukianova OA, O'Shea VL, David SS, Barton JK. Biochemistry. 2005; 44:8397–8407. [PubMed: 15938629]

14. Mui TP, Fuss JO, Ishida JP, Tainer JA, Barton JK. J. Am. Chem. Soc. 2011; 133:16378–16381. [PubMed: 21939244]

15. Grodick MA, Segal HM, Zwang TJ, Barton JK. J. Am. Chem. Soc. 2014; 136:6470–6478. [PubMed: 24738733]

16. O'Brien E, Holt ME, Thompson MK, Salay LE, Ehlinger AC, Chazin WJ, Barton JK. Science. 2017; 355:813.

17. Porello SL, Cannon MJ, David SS. Biochemistry. 1998; 37:6465–6475. [PubMed: 9572864]

18. Fan L, Fuss JO, Cheng QJ, Arvai AS, Hammel M, Roberts VA, Cooper PK, Tainer JA. Cell. 2008; 133:789–800. [PubMed: 18510924]

19. Ren B, Duan X, Ding H. J. Biol. Chem. 2009; 284:4829–4835. [PubMed: 19074432]

20. Weiner BE, Huang H, Dattilo BM, Nilges MJ, Fanning E, Chazin WJ. J. Biol. Chem. 2007; 282:33444–33451. [PubMed: 17893144]

21. Gorodetsky AA, Boal AK, Barton JK. J. Am. Chem. Soc. 2006; 128:12082–12083. [PubMed: 16967954]

22. Bartels PL, Zhou A, Arnold AR, Nuñez NN, Crespilho FN, David SS, Barton JK. Langmuir. 2017; 33:2523–2530. [PubMed: 28219007]

23. Ha Y, Arnold AR, Nuñez NN, Bartels PL, Zhou A, David SS, Barton JK, Hedman B, Hodgson KO, Solomon EI. J. Am. Chem. Soc. 2017; 139:11434–11442. [PubMed: 28715891]

24. Yavin E, Boal AK, Stemp EDA, Boon EM, Livingston AL, O'Shea VL, David SS, Barton JK. Proc. Natl. Acad. Sci. U. S. A. 2005; 102:3546–3551. [PubMed: 15738421]

25. Dey A, Jenney FE, Adams MWW, Babini E, Takahashi Y, Fukuyama K, Hodgson KO, Hedman B, Solomon EI. Science. 2007; 318:1464–1468. [PubMed: 18048692]

26. Arnold AR, Grodick MA, Barton JK. Cell Chem. Biol. 2016; 23:183–197. [PubMed: 26933744]

27. Tse ECM, Zwang TJ, Barton JK. J. Am. Chem. Soc. 2017; 139:12784–12792. [PubMed: 28817778]

28. Pheeney CG, Arnold AR, Grodick MA, Barton JK. J. Am. Chem. Soc. 2013; 135:11869–11878. [PubMed: 23899026]

29. Greeley RS, Smith WT, Stoughton RW, Lietzke MH. J. Phys. Chem. 1960; 64:652–657.

30. Burgers PMJ, Yoder BL. J. Biol. Chem. 1993; 268:19923–19926. [PubMed: 8104181]

31. Garg P, Stith CM, Sabouri N, Johansson E, Burgers PM. Genes Dev. 2004; 18:2764–2773. [PubMed: 15520275]

32. Kissinger, PT., Heineman, WR. Laboratory Techniques in Electroanalytical Chemistry 2nd ed. Kissinger, PT., Heineman, WR., editors. Marcel Dekker; New York: 1996. p. 51-139.

33. Stodola JL, Burgers PM. Nat. Struct. Mol. Biol. 2016; 23:402–408. [PubMed: 27065195]

34. Schaefer KN, Barton JK. Biochemistry. 2014; 53:3467–3475. [PubMed: 24853816]

35. Johnson RE, Prakash L, Prakash S. Methods Enzymol. 2006; 408:390–407. [PubMed: 16793382]

36. Tomoaki O, Nakamura H, Katsumi N, Cusanovich MA, Aktus H. Biophys. J. 1998; 75:1483–1490. [PubMed: 9726950]

37. Lode ET, Murray CL, Rabinowitz JC. J. Biol. Chem. 1976; 251:1683–1687. [PubMed: 3503]

38. Johansson E, Majka J, Burgers PM. J. Biol. Chem. 2001; 276:43824–43828. [PubMed: 11568188]

39. Boon EM, Salas JE, Barton JK. Nat. Biotechnol. 2002; 20:282–286. [PubMed: 11875430]

40. Kelley SO, Barton JK, Jackson NM, Hill MG. Bioconjug. Chem. 1997; 8:31–37. [PubMed: 9026032]

41. Sweeney WV, Rabinowitz JC. Annu. Rev. Biochem. 1980; 49:139–161. [PubMed: 6250442]

42. Johnson MK, Duderstadt RE, Duin EC. Adv. Inorg. Chem. 1999; 47:1–82.

43. Duff JLC, Breton JLJ, Butt JN, Armstrong FA, Thomson AJ. J. Am. Chem. Soc. 1996; 118:8593–8603.

44. Hedglin M, Pandey B, Benkovic SJ. Proc. Natl. Acad. Sci. 2016:201523653.

45. Kulak NA, Pichler G, Paron I, Nagaraj N, Mann M. Nat. Methods. 2014; 11:319–324. [PubMed: 24487582]

46. Goffeau A, Barrell BG, Bussey H, Davis RW, Dujon B, Feldmann H, Galibert F, Hoheisel JD, Jacq C, Johnston M, Louis EJ, Mewes HW, Murakami Y, Philippsen P, Tettelin H, Oliver SG. Science. 1996; 274:546–567. [PubMed: 8849441]

47. Lengronne A, Pasero P, Bensimon A, Schwob E. Nucleic Acids Res. 2001; 29:1433–1422. [PubMed: 11266543]

48. Henderson PT, Jones D, Hampikian G, Kan Y, Schuster GB. Proc. Natl. Acad. Sci. U.S.A. 1999; 96:8353–8358. [PubMed: 10411879]

49. Armitage B, Yu C, Devadoss C, Schuster GB. J. Am. Chem. Soc. 1994; 116:9847–9859.

50. Gasper SM, Schuster GB. J. Am. Chem. Soc. 1997; 119:12762–12771.

51. Nuñez ME, Hall DB, Barton JK. Chem. Biol. 1999; 6:85–97. [PubMed: 10021416]

52. Berti M, Vindigni A. Nat. Struct. Mol. Biol. 2016; 23:103–109. [PubMed: 26840898]

53. De Piccoli G, Katou Y, Itoh T, Nakato R, Shirahige K, Labib K. Mol. Cell. 2012; 45:696–704. [PubMed: 22325992]

54. Zeman MK, Cimprich KA. Nat. Cell Biol. 2014; 16:2–9. [PubMed: 24366029]

55. Saldivar JC, Cortez D, Cimprich KA. Nat. Rev. Mol. Cell Biol. 2017; 18:622–636. [PubMed: 28811666]

56. Azzam EI, Jay-Gerin JP, Pain D. Cancer Lett. 2012; 327:48–60. [PubMed: 22182453]

57. McCulloch SD, Kokoska RJ, Garg P, Burgers PM, Kunkel TA. Nucleic Acids Res. 2009; 37:2830–2840. [PubMed: 19282446]

58. Zellweger R, Dalcher D, Mutreja K, Berti M, Schmid JA, Herrador R, Vindigni A, Lopes M. J. Cell Biol. 2015; 208:563–579. [PubMed: 25733714]

59. Thangavel S, Berti M, Levikova M, Pinto C, Gomathinayagam S, Vujanovic M, Zellweger R, Moore H, Lee EH, Hendrickson EA, Cejka P, Stewart S, Lopes M, Vindigni A. J. Cell Biol. 2015; 208:545–562. [PubMed: 25733713]

60. Nimonkar AV, Genschel J, Kinoshita E, Polaczek P, Campbell JL, Wyman C, Mdrich P, Kowalczykowski SC. Genes Dev. 2011; 25:350–362. [PubMed: 21325134]

61. Markkanen E, Dom J, Hübscher U. Front. Genet. 2013; 4:18. [PubMed: 23450852]

62. Baranovskiy AG, Lada AG, Siebler HM, Zhang Y, Pavlov YI, Tahirov TH. J. Biol. Chem. 2012; 287:17281–17287. [PubMed: 22465957]

63. Johnson RE, Prakash L, Prakash S. Proc. Natl. Acad. Sci. U. S. A. 2012; 109:12455–12460. [PubMed: 22711820]
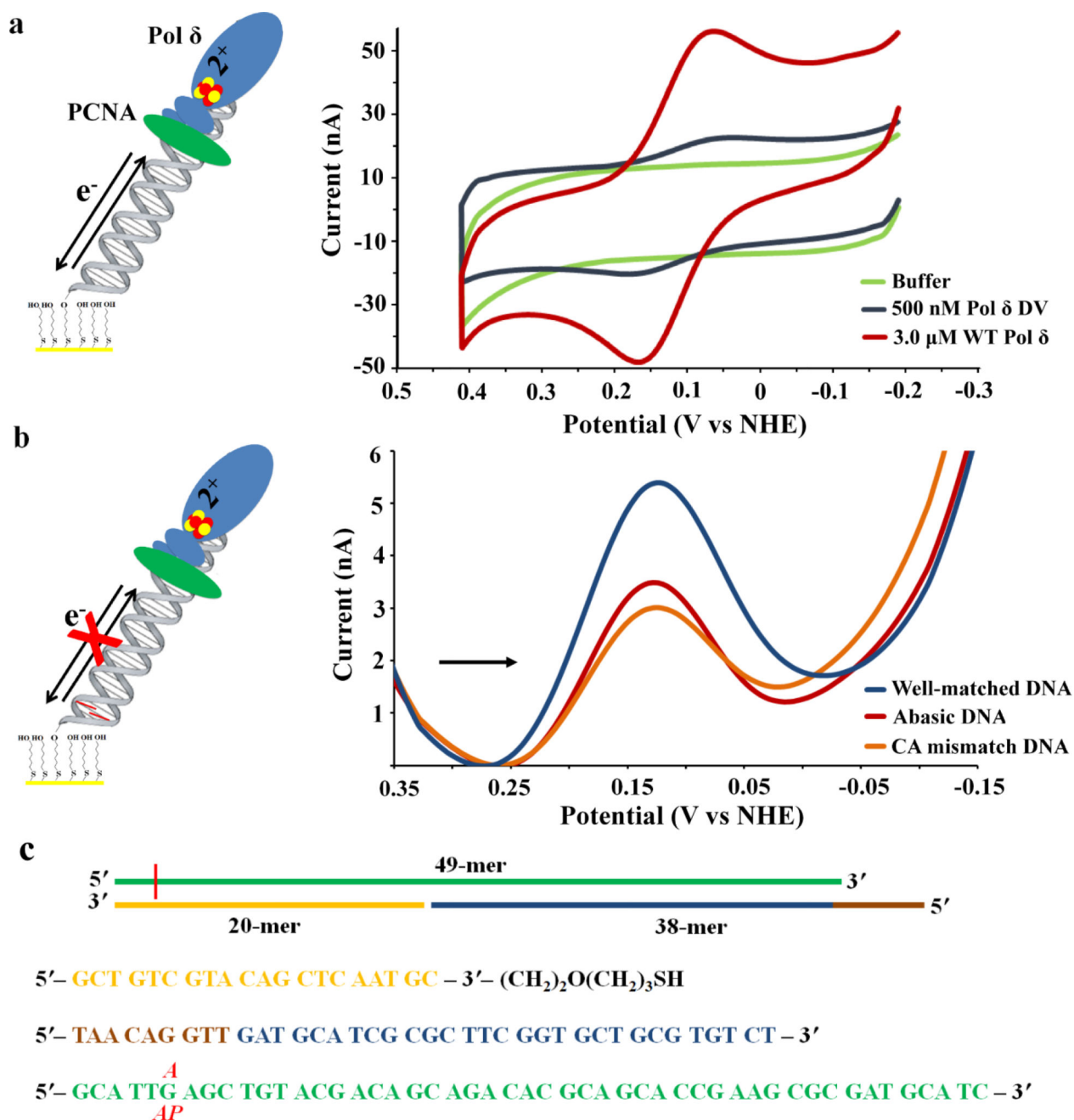
Figure 1.
Electrochemical characterization of Pol δ. (**a**) The addition of 3.0 μM WT Pol δ and 10 μM PCNA to a DNA-modified gold electrode results in a reversible CV signal with a midpoint potential centered at 113 ± 4.7 mV versus NHE (red). The exonuclease deficient mutant Pol δ DV cannot degrade DNA in the presence of catalytic magnesium, and, by including MgAc₂ and with 5 μM PCNA and excess dATP, signals at the same potential as WT can be obtained at concentrations as low as 500 nM (blue). (**b**) When an abasic site or CA mismatch is incorporated into the DNA substrate 6 nucleotides from the tethered end, signals from 500 nM Pol δ DV are attenuated by ~40 % by SQWV relative to those on well-

matched DNA, confirming that Pol δ is capable of DNA mediated signaling. (**c**) DNA substrate design for electrochemical experiments. The substrate consists of 3 parts, a 20-mer thiol, a 38-mer and a 49-mer complement. Notably, the nick in the phosphate backbone is not expected to interfere with CT. The red dash corresponds to the location of the abasic (AP) site or CA mismatch. Electrochemistry was performed in storage buffer (30 mM HEPES, pH 7.4, 350 mM NaAc, 1 mM DTT, 0.1 mM EDTA, 10% glycerol v/v, 0.01% decaethylene glycol monododecyl ether v/v), and the abasic site/mismatch discrimination experiments also included 5.0 μM PCNA, 80 μM dATP, and 8.0 mM MgAc$_2$. The CV scan rate was 100 mV/s. SQWV scans were taken at 15 Hz frequency and 25 mV amplitude, and the arrow indicates the direction of the scan.
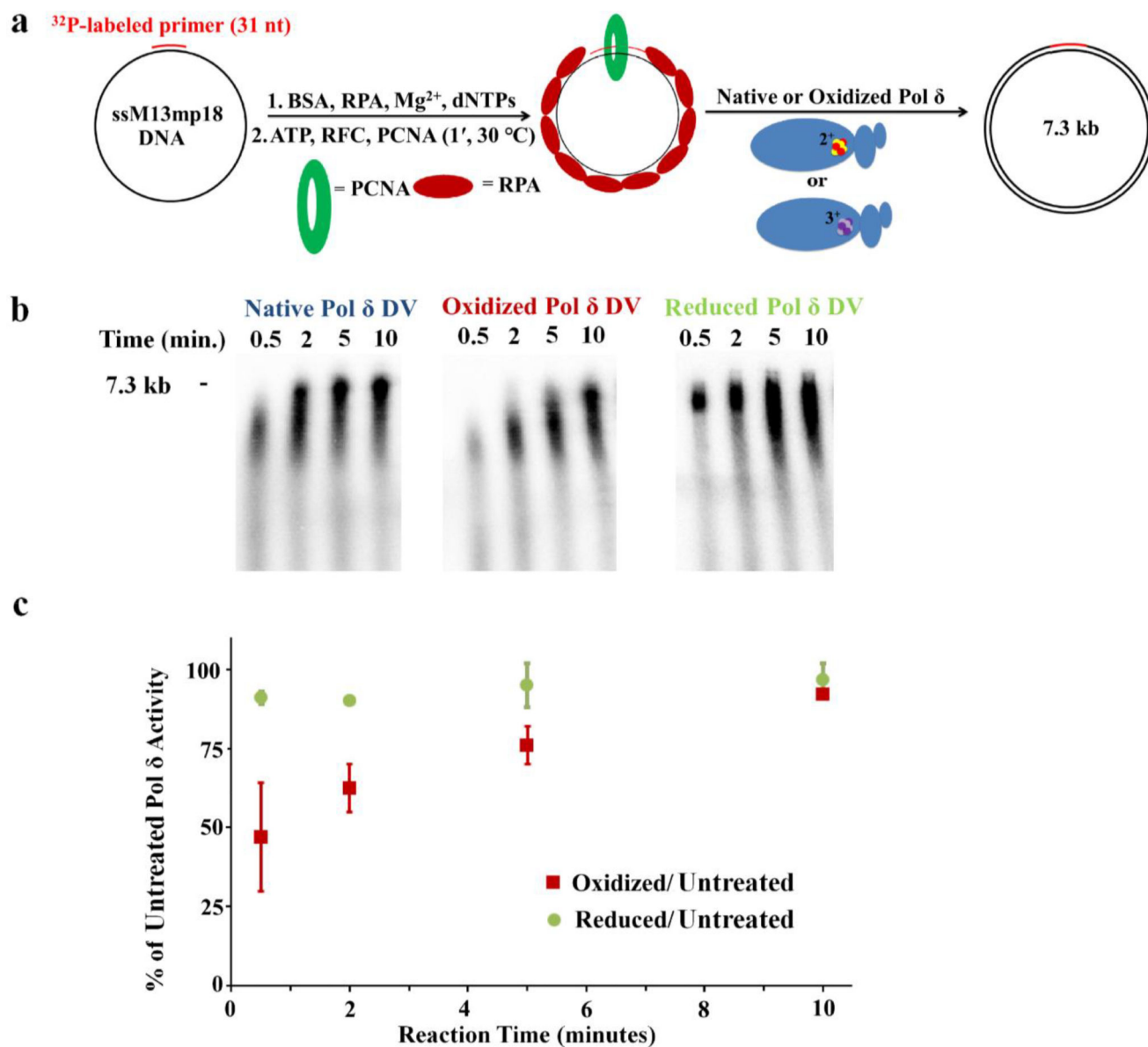
Figure 2.
Activity assays with native and electrochemically oxidized Pol δ DV. (**a**) 190 nM Pol δ DV was oxidized or reduced by bulk electrolysis at potentials of 0.412 V and −0.188 V and subsequently diluted to 2 nM final concentration into reaction mixes containing radiolabeled M13mp18 DNA. (**b, c**) As seen on representative 1% alkaline agarose gels, oxidation lowers activity levels at early time points, while reduction restores activity to native levels. The degree of this effect can be quantified by dividing the amount of DNA synthesis in reactions with oxidized or reduced Pol δ by that from reactions with untreated enzyme. The oxidation yield for the gel shown in **b** is ~80%. Error bars are standard deviation of the mean (n ⩾ 3).
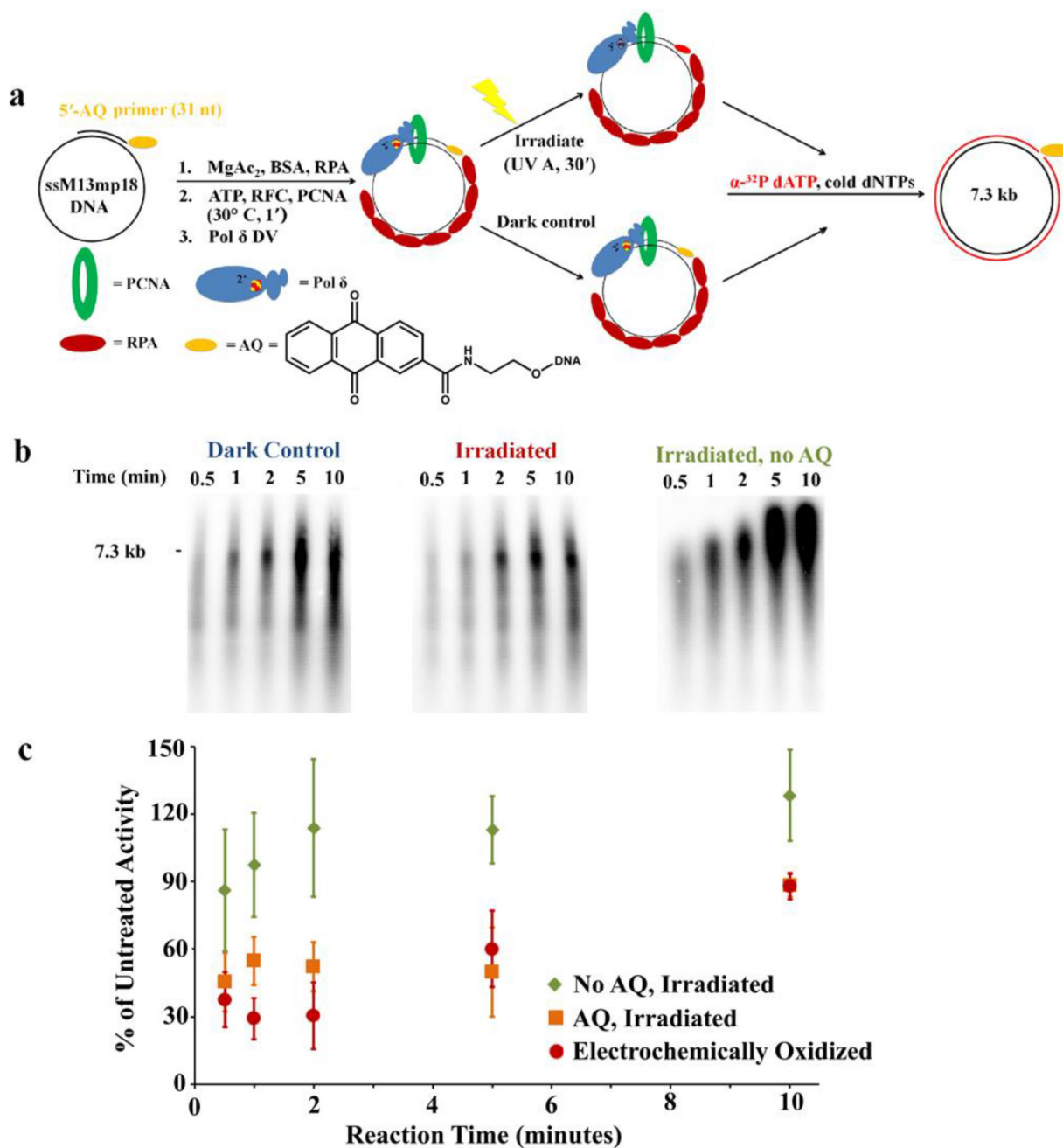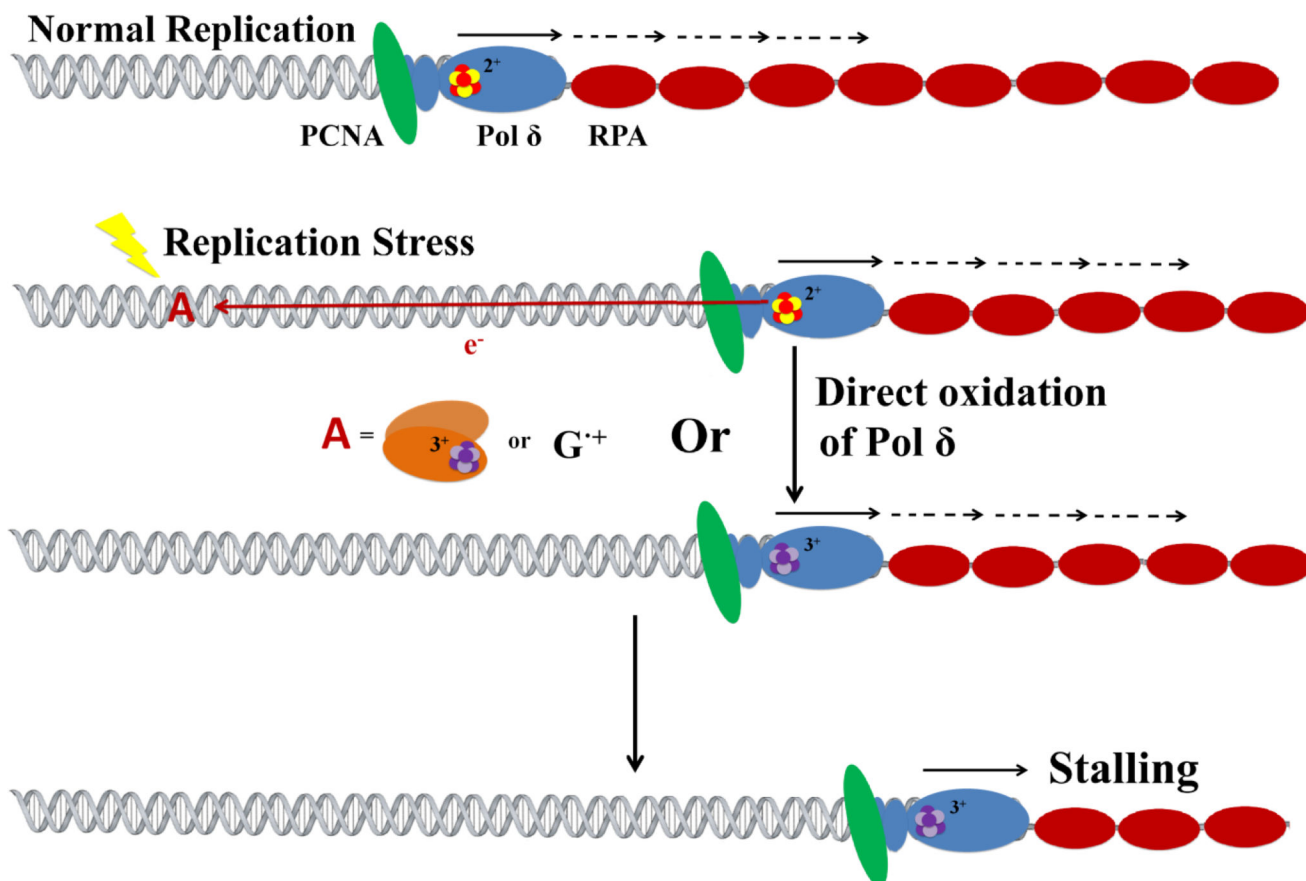
Figure 3.
Pol δ activity assays with an AQ photooxidant. (**a**) Pol δ DV was added to a reaction mix lacking dNTPs and either irradiated under a solar simulator (UVA) or left in the dark, after which dNTPs (including [α-^{32}P] dATP) were added to start the reaction. (**b, c**) 1% alkaline agarose gels show less DNA synthesis by irradiated Pol δ at early time points, matching the pattern of electrochemical oxidation. Irradiation in the absence of AQ resulted in no significant effects, indicating that AQ was oxidizing the cluster. This pattern is apparent in relative radioactivity counts (or gel quantification for electrochemical oxidation), which

further emphasize the similarity between oxidation methods. Error bars are standard deviation of the mean (n   3).

Figure 4.
A model for redox-mediated regulation of Pol δ activity. Under ordinary circumstances, Pol δ forms a complex with PCNA and processively extends lagging strand DNA (top). When replication stress occurs, lagging strand synthesis could be stalled either by transfer of an electron from the Pol δ $[4Fe4S]^{2+}$ cluster to an acceptor (**A**) or by direct oxidation of the DNA-bound Pol δ-PCNA complex. In the case of DNA-mediated oxidation, the electron acceptor could be an oxidized [4Fe4S] protein or a guanine radical cation, $G^{·+}$, formed during oxidative stress. Once the cluster is oxidized to the $[4Fe4S]^{3+}$ form, Pol δ binds more tightly to DNA and synthesis slows. After damage resolution, lagging strand replication could be restored by reduction of the $[4Fe4S]^{3+}$ cluster by another [4Fe4S] proteins.